Degradation and failure of carbon nanotube field emitters

Jean-Marc Bonard* and Christian Klinke
Institut de Physique des Nanostructures, Faculté des Sciences de Base, Ecole Polytechnique Fédérale de Lausanne, CH-1015 Lausanne EPFL, Switzerland

Kenneth A. Dean and Bernard F. Coll
Physical Sciences Research Laboratory, Motorola, 7700 South River Parkway, Tempe, Arizona 85284
(Received 29 August 2002; revised manuscript received 19 December 2002; published 17 March 2003)

The failure of individual multiwall carbon nanotubes during field emission and two-probe characterization was studied in a scanning electron microscope on emitters grown by chemical vapor deposition. The failures induced by high currents during two-probe measurements led to a sundering of the tube in or near its middle, which is consistent with a local evaporation due to resistive heating. Conversely, failures during field emission occurred at or near the substrate-emitter contact. We show that the degradation is due to mechanical failure of the contact at low applied fields, and to resistive heating (probably enhanced by the mechanical stress) at high emitted currents.

DOI: 10.1103/PhysRevB.67.115406 PACS number(s): 79.70.+q, 68.37.Hk, 81.07.De

I. INTRODUCTION

The use of carbon nanotubes as electron field emitters has been demonstrated in a variety of devices. While flat panel displays based on nanotubes[1–3] may one day claim a share of a very large market, other applications are just as promising. Let us mention high brightness sources for electron microscopes,[4] small area cathode ray tubes as giant display pixel elements,[5,6] luminescent tubes,[7] gas discharge tubes,[8] microwave amplifiers,[9] and x-ray tubes for medical imaging.[10] One of the issues for the industrial viability of the devices is the lifetime of the cathodes, and is at present poorly understood.

Few facts are currently available on the lifetime and failure of individual nanotube emitters. For arc-discharge grown multiwall nanotubes, stable emission was measured during more than two months at 0.4 μA emitted current without any observable degradation.[11] The reported cases of failure involved either an abrupt failure[12] or a gradual degradation of the walls[13] with sustained currents of up to 0.2 mA.[12,13] A gradual decrease of field enhancement due to field evaporation was also found on singlewall nanotubes when the emitted current was increased beyond a given limit (300 nA to 1 μA),[14] or when a partial pressure of O_2 was introduced in the chamber.[15] A shortening of the emitter at currents of 50–120 nA was also found on multiwall nanotubes grown by chemical vapor deposition (CVD).[16] In contrast to the gradual degradation of nanotube emitters, the phenomena leading to abrupt failure have not yet been documented. We aim here to provide some answers to this issue with field emission measurements of individual multiwall carbon nanotubes performed with a sharp anode in a scanning electron microscope (SEM).[16,17]

The experimental setup is described in Sec. II. Section III compares the failures occuring during field emission (FE) and two-probe (2P) characterization when the anode is brought into contact with the nanotube tip. We examine the different mechanisms leading to nanotube failure and develop models to support our interpretation in Sec. IV. Section V discusses the implications of our findings on practical devices, while Sec. VI presents our main conclusions.

II. EXPERIMENTAL SETUP

The studied emitters are sparse films of thin multiwalled carbon nanotubes grown by hot-filament CVD over nanosupported Ni (Ref. 18) or Fe (Ref. 19) catalysts. Such a catalyst consists of a 300-nm-thick film with bulk metallic conductivity in which the Ni or Fe catalyst nanoparticles are embedded. The catalyst is delivered onto a Si or glass substrate by sputtering[18] or microcontact printing.[19] The hot-filament CVD is performed at a substrate temperature of 570 °C under a hydrogen and methane atmosphere for 15 min.

The nanotube film is mounted on the sample holder of the SEM and is positioned at a given distance d and position with respect to anode and electron beam.[16,17] As anodes we use commercially available etched W needles with a radius of curvature of typically 1 μm. As shown in the SEM micrograph of Fig. 1(a), electrical connections allow to apply a potential difference V and to measure the collected current I between the two electrodes. The contamination effects due to SEM observation, especially before field emission, have been reduced to a minimum by using low acceleration voltage (5 kV), beam current, and magnification (below 20 k×). The electron beam was systematically blanked off during the measurements. The field emission $I-V$ characteristics were acquired with a Keithley 237 source-measure unit with a 10-ms acquisition time.

III. RESULTS

A. Field emission failure

A typical example of a field emission measurement leading to the failure of the emitter is shown in Fig. 1 for a nanotube of length $h=0.66$ μm and radius $r=5$ nm. The $I-V$ curve is given in Fig. 1(c): field emission is observed for voltages higher than 60 V, and a saturation appears around 90 V and 920 nA. The current continues to increase with the voltage, until an abrupt and irreversible drop in the

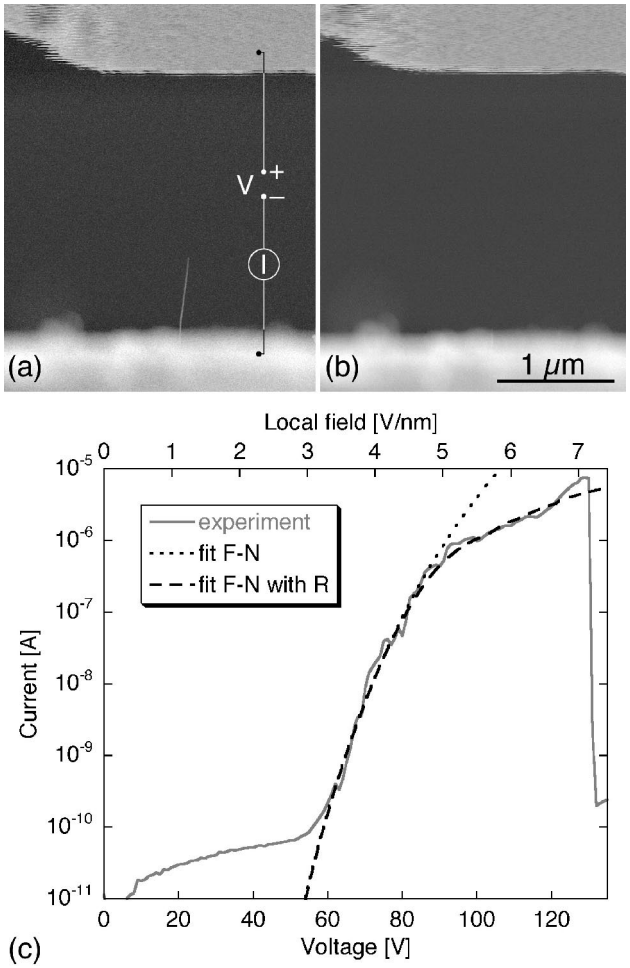

FIG. 1. (a) and (b) SEM micrograph of a nanotube of 0.66-μm length and 5-nm radius with the anode positioned at 2-μm distance before (a) and after (b) the destruction of the tube. (c) Corresponding $I-V$ curve with the best fit to the FN model [Eq. (1) $\gamma=110\pm20$, $A=3\times10^{-15}$ m^2] in dotted line and to the F-N model with series resistance in dashed line ($R=5$ MΩ).

current at 7.5 μA. The SEM micrograph of Fig. 1(b), taken after the event, shows that the emitting nanotube has disappeared.

Also shown in Fig. 1(c) is the fit of the $I-V$ curve to the Fowler-Nordheim (FN) model.[20] The FN model (with image charge correction) states that the current I (A) per emitter varies with the local field at the emitter surface F (V/m) as[20,21]

$$I=f_{\mathrm{F-N}}(V)$$
$$=A\frac{1.5\times10^{-6}}{\phi}\left(\frac{V}{d}\right)^2\gamma^2\exp\left(\frac{10.4}{\sqrt{\phi}}\right)\exp\left(\frac{-6.44\times10^{9}\phi^{1.5}d}{\gamma V}\right), \quad (1)$$

where A has the dimension of an area (m^2) and represents, in a first approximation, the emitting area; the work function ϕ is in eV, the field enhancement factor γ is defined as $F=\gamma V/d$, where V is the applied voltage; and d the interelectrode distance. With ϕ taken equal to 5.1 eV, from Fig. 1(c) we extract a field enhancement factors of $\gamma=110\pm20$ and $A=3\times10^{-15}$ m^2. The obtained fit also closely follows the measured characteristics up to the saturation.

This saturation behavior has been observed on individual multiwall[12] and single-wall[22] nanotubes, and to a lesser extent on nanotube films.[12] It was ascribed to the presence of adsorbates that enhance field emission at low fields.[22] Increasing the field beyond a given limit displaces the adsorbates (leading to fluctuations in emission current) and finally removes them. $I-V$ curves acquired immediately after such a cleaning show higher onset fields but no saturation. In every case, the absorbate could be removed either by increasing the temperature to 700 °C (Ref. 23) or by increasing the applied field by typically 30%.[22]

In our case, however, we did not observe this behavior as the saturation persisted even after doubling the applied field (the $I-V$ curves displayed in Figs. 2 and 8 show a saturation up to fields at least 40% above its onset). Another possibility is that the flattening is due to the presence of a large resistance R in series with the emitter (e.g., at the nanotube-substrate contact). In that case, the voltage drop $U=RI$ across the resistance will lead to a decrease of the effective applied voltage, and therefore to a flattening of the characteristics.[24] Including the effect of a series resistance in the FN equation is not trivial. Instead, the $I-V$ curves can be numerically fitted by solving numerically the equation system $\{I=f_{\mathrm{FN}}(V-U);\ U=RI\}$, as has been done here. This allows to reproduce the saturation behavior, as shown on Fig. 1 for $R=5$ MΩ (note that including a series resistance in the model does not change the extracted values of γ and A).

B. Two-probes failure

In Fig. 2 we show a second example that illustrates another type of nanotube failure, namely during electrical characterization in 2P configuration. The emission sets in at 112 V in the initial situation of Fig. 2(a), follows the FN law and saturates markedly at 160 V and 50 nA. The anode was then lowered into contact with the nanotube [Fig. 2(b)] to perform 2P measurements. The nanotube failed at 4 V and 20 μA, as can be seen in Fig. 2(c), where the two parts remain attached to cathode and anode, respectively. Field emission on the remaining segment [Fig. 2(d)] sets in at 43 V, and follows the FN law up to the failure of the emitter [Fig. 2(e)] at 108 V and 9 μA. Note that the emission voltages and γ factors cannot be directly compared as the interelectrode distance and tube length are not the same for the two $I-V$ curves of Fig. 2(f).

Figure 2 shows that the nanotube is severed at or near its middle in 2P failure, which has been observed in all cases. Conversely, the nanotube is most often completely removed from the substrate in FE failure (a short stub of less than 100 nm remained in a few cases).

C. Failure at low versus high currents

To investigate in more detail the cause(s) of abrupt emitter failure, in Fig. 3 we display some relevant parameters for both 2P and FE failures, in particular the current I_{f}, voltage V_{f}, and (for FE failure) the field $F_{\mathrm{f}}=\gamma V_{\mathrm{f}}$ at which the failure

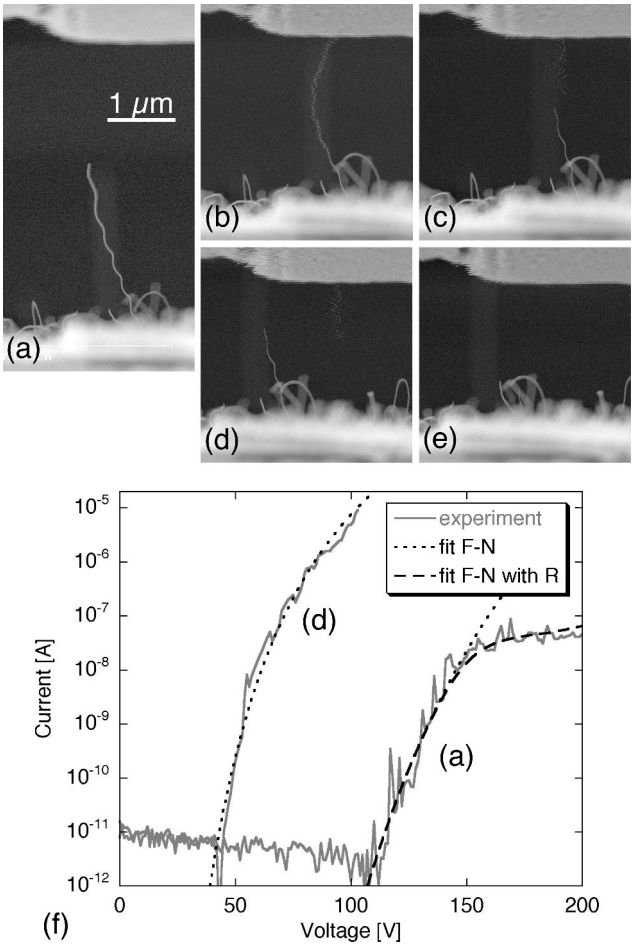

FIG. 2. (a)-(e) SEM micrographs of a nanotube with (f) corresponding $I-V$ curves acquired in the configurations shown in (a) and (d). (a) shows the nanotube of 2.35-μm length and 7-nm radius with the anode positioned at 3.75 μm distance before field emission, (b) in contact with the anode before 2P measurements, (c) after 2P failure, and (d) subsequent lateral displacement of the anode for field emission. The nanotube now has a length of 1.32 μm with the anode positioned at 2-μm distance. (e) shows the situation after FE failure. (f) gives also the best fit to the FN model [$\gamma=70$ for (a) and $\gamma=150$ for (d)] with the dotted line to the FN model with the series resistance with the dashed line [$R=200$ MΩ for (a)].

occurred. FE failure occurred at currents between $I_f=2$ nA and 9 μA, and at voltages between $V_f=103$ and 166 V, which corresponds to fields $F_f=3-10$ V/nm (with γ obtained from the FN fits). Interestingly (but not unexpectedly), the failure field increases with the failure current. When the failure occurs between $I_f=1$ nA and 1 μA, F_f is in the range 3–4.6 V/nm, as compared to $F_f=5-10$ V/nm for I_f between 1 and 10 μA.

Conversely, the failure currents for 2P measurements were consistently high, between $I_f=5$ and 50 μA, with far lower applied voltages of $V_f=2-11$ V leading to a power at failure between 20 and 200 μW. The $I-V$ behavior is linear at low voltages, with estimated contact resistances between 300 kΩ and 400 MΩ, which is quite typical of 2P measurements.[25,26] It is worth noting that the 2P resistance of

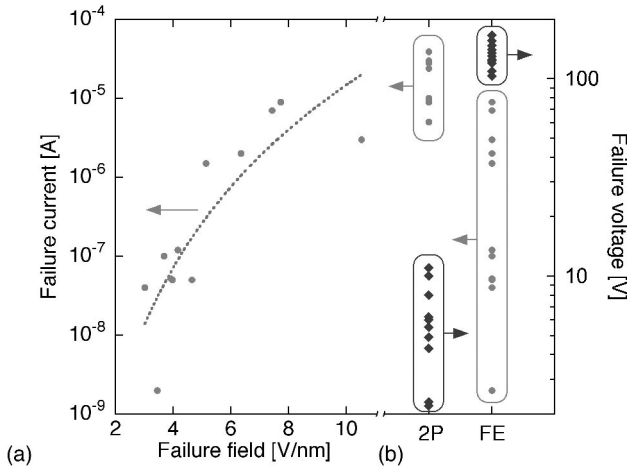

FIG. 3. (a) Failure current I_f as a function of the failure field $F_f=\gamma V_f$ (γ has been estimated with the FN law, and the dotted line is a guide for the eye). (b) I_f (circles, left axis) and V_f (diamonds, right axis) for 2P and FE failures, respectively.

catalyst layer and substrate (measured with the anode in nanotube-free regions) is typically 20 kΩ, indicating that the resistance values obtained in 2P are mostly due to the contacts and nanotube.

IV. FAILURE MECHANISMS

A. Gradual failure

A gradual degradation of nanotube emitters has been observed in the past during experiments at constant applied voltage.[13,14,16,27] On single-wall nanotubes, the degradation was related either to field evaporation,[14] to ion bombardment from the gas phase, or to selective oxidation.[27] On multiwall nanotubes, a shortening of the emitter over time[16] or damage to the outer walls of the nanotube due to high currents[13] was observed. Note that the phenomena observed on single-wall nanotubes are probably also involved in the degradation of multiwall nanotubes (MWNTs), but no relevant experiments on MWNTs have to our knowledge been reported. We did not perform measurements at constant applied voltage in the course of the present SEM study. We will therefore not address further these gradual phenomena as the failure of the emitters was always abrupt.

B. Two-probe failure

A Nanotube characterization and degradation during 2P and 4P measurements were reported by several groups. Collins *et al.* observed that arc-discharge multiwall nanotubes can be degraded shell by shell under carefully controlled conditions, so that only the outer conducting wall fails at 10−100 μA.[28] These currents are comparable to the maximal values obtained during field emission (100−200 μA) for the same type of nanotubes.[12] Interestingly, the behavior of nanotubes grown directly by CVD is different, as shown in Figs. 3(a) and 3(b): the failure current is systematically higher for 2P measurements by as much as three orders of magnitude. This has also been observed on plasma-enhanced

CVD-grown fibers[29] of 50-nm diameter that failed around $I_f = 10-20$ μA under FE,[30] and at around $I_f = 0.2-2$ mA in 2P measurements.[31]

In 2P measurements, the nanotube (or the outer shell) is ruptured near the middle[28] or at a weak point.[32] This suggests that the tube is resistively heated and that the temperature becomes locally high enough to enhance oxydative ablation of the tube or even to vaporize the graphitic wall. The resistances we measured (300 kΩ to 400 MΩ) are typical for 2P characterization,[25] but have to be compared with the intrinsic resitivity of the nanotube. Bachtold *et al.* measured 10 kΩ/μm for arc-discharge multiwall nanotubes,[33] while Ahlskog *et al.* found values higher by one order of magnitude for CVD-grown multiwall nanotubes (between 40 and 110 kΩ/μm, due to the higher defect density in CVD-grown nanotubes).[34] It can safely be assumed that the contact resistance is invariably far higher than the resistance of the nanotube for the typical emitter lengths considered here ($0.4-4$ μm), which is quite typical in 2P measurements.

One can therefore simplify the system in 2P measurements as three resistances in series, namely, the two substrate- (respectively anode-) nanotube contact resistances and the resistance of the nanotube proper. As the resistance of the system is dominated by the contacts, there is also no significant dependence of the nanotube length or diameter on the failure current or power or on the 2P resistance. Usually, the two contact resistances are neglected as the substrate and anode act as heat sinks (even though they dissipate far more power than the resistance of the tube; see Sec. IV D).

The temperature can be estimated analytically when only the emitter dissipates power. Dolan *et al.* showed, for a cylindrical emitter, that the temperature increases with increasing distance to the contact x as $h^2-(x-h)^2$.[35] The highest temperature is reached at the emitting end, and amounts to

$$\Delta T_{\max} = \frac{\rho h^2 I^2}{2\pi^2 r^4 \kappa} = \frac{RhI^2}{2\pi r^2 \kappa}, \tag{2}$$

where $\Delta T_{\max} = T - T_0$, T_0 is the substrate temperature, and ρ and κ are the electrical and thermal conductivities of the emitter, with $R = \rho h/\pi r^2$. For the 2P case, the temperature is highest in the middle of the nanotube, and amounts to

$$\Delta T_{\max} = \frac{\rho h^2 I^2}{8\pi^2 r^4 \kappa} = \frac{RhI^2}{8\pi r^2 \kappa}. \tag{3}$$

It is worth noting that the occurrence of heating during nanotube field emission was recently confirmed by two groups.[36,37] In particular, field emission energy distribution measurements suggest a temperature of 2000 K at the apex of the nanotube at 1-μA emitted current.[36]

The main problem in estimating $\Delta T_{\max}$ is to find reliable values for κ and R (or ρ) and for their dependence in temperature. R has been lately measured for CVD-grown nanotubes and has been shown to vary from one tube to the next by as much as a factor 3.[34] As for κ, values of 3000 (Ref. 38) and 25 W/m K (Ref. 39) have been reported for a single arc-discharge multiwall nanotube and for a CVD-grown nanotube film, respectively. Taking a mean value of $R = 50$ kΩ/μm and $\kappa = 25$ W/m K, from Eq. (3) we estimate a temperature difference between 50 and 3000 K for the observed 2P failures. Taking into account the fact that R may vary from tube to tube and that r is overestimated in SEM, these values are in the expected range for a heat failure. We will also see in Sec. IV D that this temperature may even be substantially higher if some heat is dissipated at the contact.

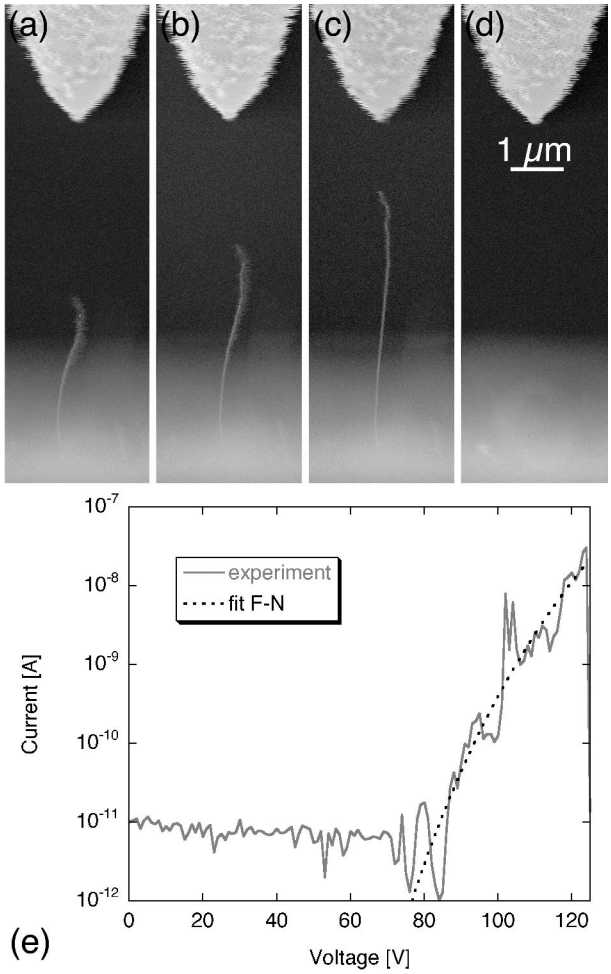

FIG. 4. (a)–(d) SEM micrographs of a nanotube of 4.56-μm length and 5-nm radius with the anode positioned at 5.8-μm distance at (a) 0-, (b) 2-, and (c) 4-V applied voltage before and (d) after destruction of the tube. (e) Corresponding $I-V$ curve with the best fit to the FN model ($\gamma = 220$) shown by the dotted line.

C. Field emission failure: low currents

Though resistive heating is likely to be the main cause for 2P failure, it is doubtful that it plays a role in all FE failures. I_f is scattered over more than three orders of magnitude (see Fig. 3) and $\Delta T_{\max}$ [as estimated from Eq. (2)] is in the range 40–920 K for the high current failures ($I_f \geqslant 1$ μA), while it is below 1 K for FE failures at lower currents. We argue below that the cause of the latter type of failures is probably of mechanical origin.

The SEM micrographs of Fig. 4 reveal that even a small applied voltage (e.g., 2 V) is sufficient to significantly deflect the nanotubes. The emitters are also aligned perpendicular to

the substrate at typically a quarter of the voltage necessary for field emission regardless of their initial alignment. The electrostatic force applied on the nanotubes during field emission can also lead to irreversible changes in shape (not shown here). In fact, simple arguments show that the mechanical stress on the emitters is considerable.

The mechanical force due to the applied field $\vec{F}$ can be obtained by integrating the stress over the whole surface of the nanotube.[40] For conducting materials, the force $d\vec{T}$ on a surface element $d\vec{A}$ is $d\vec{T}=(\epsilon_0/2)\vec{F}^2\ d\vec{A}$.[40] When the nanotube is perpendicular to the substrate [which is the case during FE; see Fig. 4(c)], the problem has a cylindrical symmetry and the radial contributions to $d\vec{T}$ cancel out following integration over the whole surface of the tube. The resulting force will act at the emitting end and is directed along the axis $\hat{z}$ of the tube. The tube is therefore subjected to a pure tensile stress with

$$\vec{T} \quad = \hat{z}\int_{\text{cap}} \frac{\epsilon_0}{2}\vec{F}^2\ d\vec{A} \tag{4}$$

$$= \hat{z}\int_0^{\pi/2}\int_0^{2\pi}\frac{\epsilon_0}{2}|\vec{F}(\theta)|^2\cos(\theta)^2\ r^2\sin(\theta)d\theta\ d\phi \tag{5}$$

$$= \hat{z}\pi\epsilon_0 r^2\int_0^{\pi/2}|\vec{F}(\theta)|^2\cos(\theta)^2\sin(\theta)d\theta, \tag{6}$$

where $\vec{F}(\theta)$ takes into account the decrease of $\vec{F}$ as one moves away from the apex of the tube at $\theta=0$. As shown in Ref. 41,

$$|\vec{F}(\theta)| = \frac{\gamma V}{d}\frac{\cos(\theta)}{2}, \tag{7}$$

and hence

$$\vec{T} = \hat{z}\frac{7\pi}{24}\epsilon_0 r^2\left(\frac{\gamma V}{d}\right)^2. \tag{8}$$

Taking γ from the fit to the FN law of Eq. (1) and h and r from SEM measurements, the applied force at failure T_f and applied stress at failure $G_f=T_f/\pi r^2$ can be estimated with V_f. For the example of Fig. 4, the field strength and resulting applied force are $F=0.075$ V/nm and $T=1.1$ pN at 2 V, and $F_f=4$ V/nm and $T_f=4$ nN at failure (118 V), respectively.

The values obtained for T_f and G_f are summarized in Fig. 5 as a function of the failure current [Fig. 5(a)] and failure field [Fig. 5(b)]. The estimated force and stress at failure range between 4 and 25 nN, and 20 and 200 MPa, respectively. We find a marked dependance of stress versus current at failure in Fig. 5(a), as G_f amounts to 20–60 MPa for failures below 1 μA as compared to 60–300 MPa above 1 μA. A similar relationship with the field at failure is shown in Fig. 5(b), with the quadratic increase of the stress with the field predicted by Eq. (8). The above values are comparable to the ones measured by Semet *et al.*, who studied individual 60-nm-diameter fibers grown by plasma-enhanced CVD with scanning anode field emission microscopy (SAFEM).[30] In SAFEM,[30,42] a probe ball (or a sharp tip[42]) is scanned over the nanotube film at a constant height of a few μm. As the emitters cannot be simultaneously imaged, a direct comparison between the dimensions of the emitter and its field emission properties are more difficult than in our case (although the structures considered in Ref. 30 have very uniform spacing, length and diameter). Semet *et al.* observed sharp drops in the emission current above 20 μA, which they attributed to a mechanical degradation of the emitters. The corresponding force is estimated to 800 nN, leading to a stress of 280 MPa which is readily comparable to the highest stresses at failure observed here.

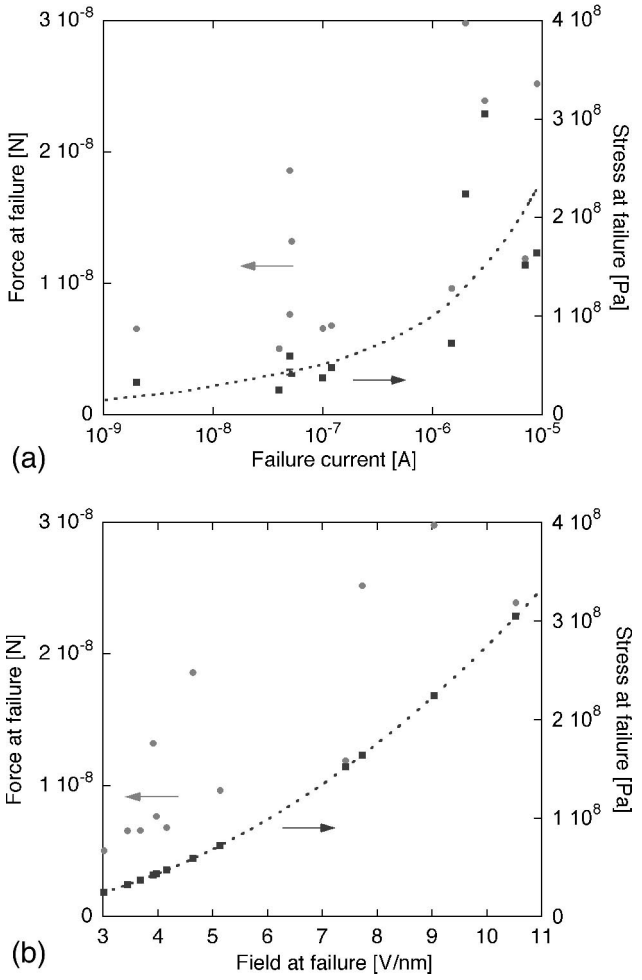

FIG. 5. Estimated force (circles, left axis) and stress (squares, right axis) at failure as a function of (a) failure current I_f and (b) field at failure F_f. The line in (a) is a guide for the eye.

It is also interesting to compare these values with the ultimate strength of a nanotube under tensile loading. The force necessary to fracture a well-anchored multiwall arc-discharge nanotube is in the 400–1400-nN range (corresponding to a stress of 20–63 GPa).[43] This is far higher than the values found in Fig. 5, even accounting for the fact that CVD-grown tubes are more defective than arc-discharge ones and that the force necessary for fracturing the nanotube will hence be lower. In our case, however, the nanotubes grow perpendicularly to the substrate, and the contact area of

the nanotubes with the support is very small, on the order of area of the catalyst particle. Conversely, the contact lies along the plane of the sharpened tip in the mechanical measurements mentioned above and covers in most cases over 1 μm of tube length, leading to far larger contact areas.[43] This is also the case in most studies of FE degradation that have been performed up to now on individual nanotubes,[12–15] where the nanotube was attached on sharpened Au wires or scanning probe microscope tips.

The emitter-substrate contact is therefore a mechanical weak point in nanotube films grown on planar substrates, and emitters may fail mechanically at applied fields and emitted currents far lower than the one necessary for electrical failure (see Sec. IV D). Interestingly, the $I-V$ characteristics of tubes with $I_f \leqslant 1$ μA were very noisy and unstable as in the case of Fig. 4, which suggests that the field emission properties were perturbed by the mechanical stressing. Also note that we have witnessed only one case (over 80 emitters) of mechanical failure prior to electron emission.

In the frame of the above argument, one could expect a better adhesion (and hence resistance to mechanical failure) with increasing nanotube radius as the contact area should increase. Interestingly, we find the inverse behavior as field and stress at failure decrease with increasing tube diameter [Fig. 6(a)]. Furthermore, nanotubes with smaller radii fail at higher currents [Fig. 6(c)] in FE, while we find no dependence on the tube radius (or length) for 2P failure. Figure 6(b) also reveals that shorter nanotubes withstand higher fields before failure. It seems therefore that, in our case, small nanotube diameters and lengths are clearly an advantage. This surprising finding is probably due to the fact that CVD-grown nanotubes tend to show more defects in the wall as their radius increases. We caution the reader that this statement cannot be generalized, as the support-emitter contact depends critically on catalyst, growth conditions, post-growth treatments, etc. Figure 6 clearly demonstrates, nevertheless, the importance of a better characterization and understanding of the emitter-substrate contact in future studies.

D. Field emission failure at high currents

Mechanical failure cannot account for all the cases we observed. In particular, several nanotubes emitted repeatedly at voltages of 300 V and fields of 8 V/nm, i.e., significantly higher than the mean failure field of 5 V/nm.

One mechanism that has been evoked for field emitter failure[44] is arcing, i.e., an arc between a cathode and an anode that is initiated by field emission. Such arcing events are also commonly observed on diamond and diamondlike carbon films, and lead to an enhancement of the field emission properties.[45,46] They are caused usually by a high field emission current,[44] anode outgassing,[45] or local evaporation of cathode material[46] that create a conduction channel between the electrodes, leading to a discharge which destroys or damages the emitter. We rule out this mechanism for several reasons. First, the applied voltage during such discharges is much higher and involves hence a larger discharge energy. Second, arcing leads to a severe damage of the emitter (such as the formation of craters or localized melting of the substrate). For example, Nilsson *et al.* observed, with a SEM, damages to nanotube films and substrates after a failure provoked in SAFEM for currents at failure above 10 μA.[47] This implies that the temperature can reach the melting temperature of Si: 1420 °C. Such damages easily extent over distances of 10 μm away from the damage center. We did not

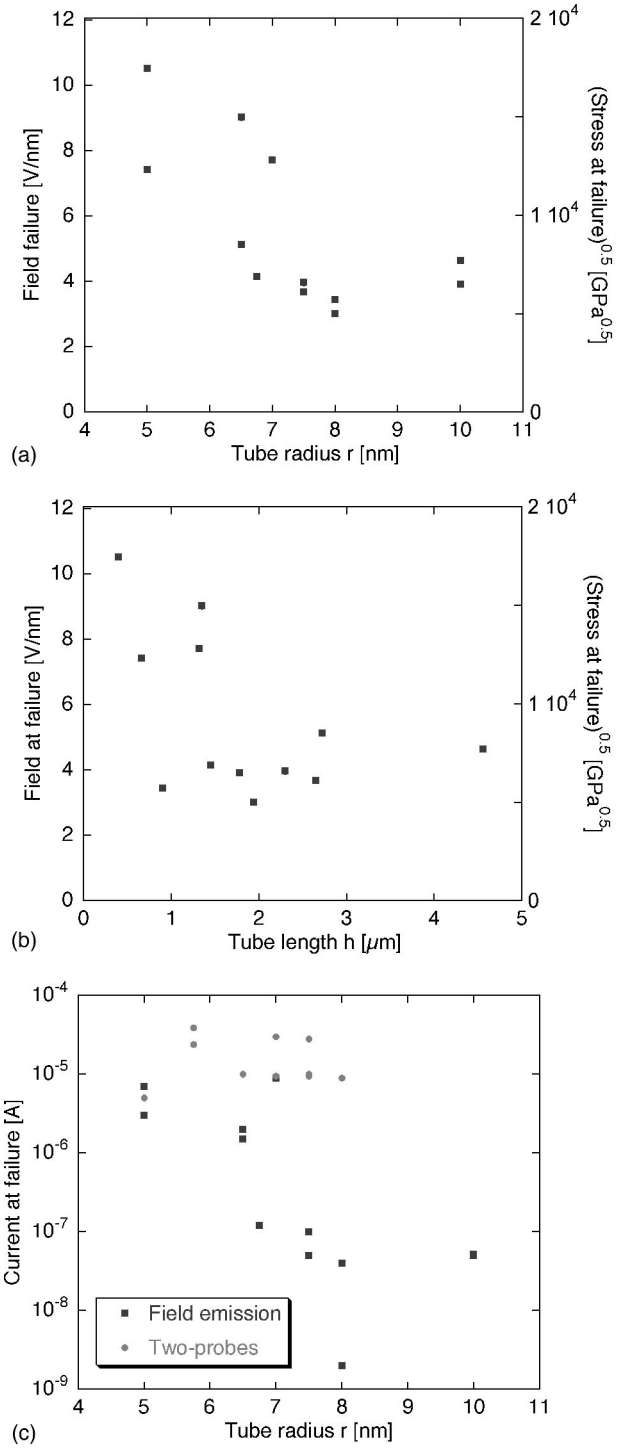

FIG. 6. (a) and (b) Failure field F_f and square root of the stress at failure $G_f^{0.5}$ as a function of (a) the tube radius and (b) the tube length. (c) Failure current I_f as a function of the tube radius for FE and 2P failures.

observe any comparable damage to film or substrate after FE failure [see, e.g, Fig. 2(e)].

Instead, we see in Fig. 3(b) that the failures at fields beyond 4 V/nm also correspond to $I_f \geqslant 1$ μA, i.e., in or near the lower range of 2P failures. We also estimate ΔT_{max} with Eq. (2) to be in the range 40–920 K for the high current failures, i.e., in the range of the estimated temperatures in 2P failure. This suggests that an increase in temperature may play a role, which at first glance seems incompatible with the fact that the failure occurs at the contact. We show below that the degradation is probably of electrical origin for the failures occuring at high currents, i.e., through a Joule heating at the contact resistance.

Equations (2) and (3) give the temperature increase due to dissipation in the nanotube only, with the assumption that no other heat sources are present and that the substrate (and the probe in 2P configuration) is a perfect heat sink. However, the contact resistance in our case is quite high, and is likely to dissipate heat in a small volume, and the catalyst, nanotube, and Si substrate have a finite thermal conductivity. It is therefore probable that not only the nanotube, but also the vicinity of the contact between nanotube and substrate, are heated during field emission.

To assess this possibility, we performed numerical simulations using the program FREEFEM+(Ref. 48) which solves partial differential equations (such as the heat diffusion equation) by the finite element method. We considered two heat sources, namely, a nanotube itself with a resistance of 50 kΩ/μm, and a contact with a resistance that dissipates heat in a spherical volume with the same radius as the nanotube, $\frac{4}{3}\pi r^3$. We took tabulated values for the density and thermal conductivity of Si and Fe,[49] and took $\kappa = 25$ W/m K for the nanotube. We also assumed that the nanotube has an internal cavity of radius $r/3$.

We make no assumptions on the nature of the contact resistance. TEM micrographs show that the nanotube is in most cases directly connected to the matrix with the metallic catalyst particle at the root of the tube, although several graphitic layers may also be intercalated. It is therefore likely that the contact resistance is localized in a small volume, especially if the resistance is high.

FREEFEM+ performs simulations in two dimensions, which means that we are not simulating a single nanotube on a surface but a dense wall of nanotubes. In a first step, we check the consistency of the simulations by neglecting the contact resistance. The profile of the temperature along the nanotube reproduces well the behavior of Eq. (2) as the temperature increases along the tube with $h^2-(x-h)^2$, where x is the distance to the contact. ΔT_{max} is also proportional to R and to r^{-2}. The only difference due to the two-dimensional (2D) character of the simulations as compared to the 3D situation considered here [and in Eq. (2)] is that we obtain a dependence of ΔT_{max} that is proportional to h instead of h^2. This also implies that the absolute value of ΔT_{max} differs from the prediction of Eq. (2) by typically a factor 5–10 times [the same observations apply to the 2P configuration and Eq. (3)]. We take this fact into account in the following by calibrating the values obtained by FREEFEM+ for a given nanotube length with Eq. (2).

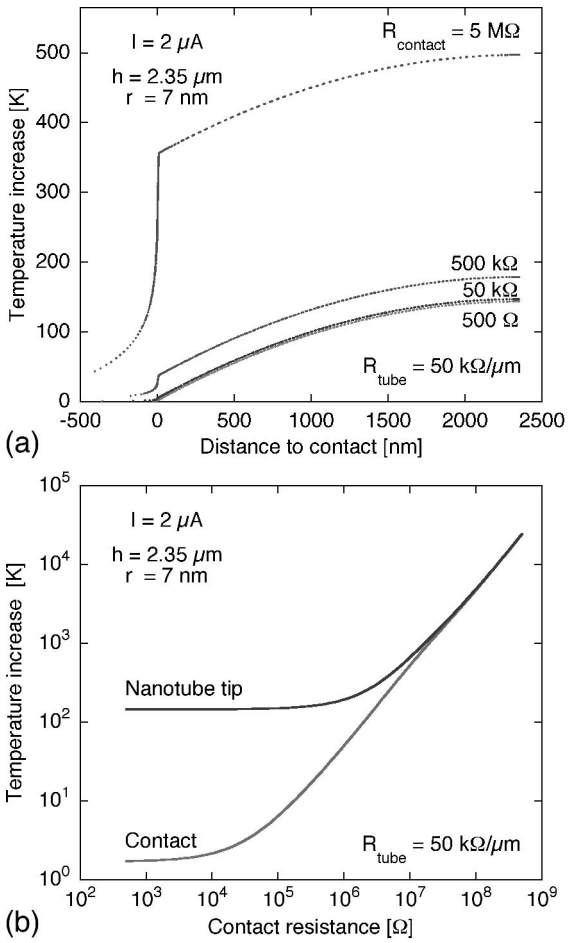

FIG. 7. (a) Temperature profile during field emission along a nanotube for varying values of the contact resistance. (b) Temperature increase during field emission at the contact and at the tip of the nanotube as a function of the contact resistance. The dimensions of the nanotube correspond to the emitter studied in Fig. 2 ($h = 2.35$ μm, $r = 7$ nm) with a resistance of 50 kΩ/μm. The emitted current has been set to 2 μA.

Figure 7(a) gives the temperature profile along the nanotube and the underlying substrate for different contact resistances. The lowermost profile corresponds to a negligible contact resistance as predicted by Eq. (2). This increase in temperature along the nanotube does not change as the contact resistance increases. For contact resistances above 500 kΩ, however, heating at the contact becomes significant and the absolute value of the temperature increases with the dissipated power. We illustrate this fact in Fig. 7(b). While the relative increase between the contact and nanotube apex is constant, the temperature difference at the contact increases linearly beyond $R_c = 500$ kΩ. Figure 7 underlines clearly that a Si substrate is not a perfect heat sink as is usually assumed (which will also be the case for glass). The temperature increase can easily reach values that lead to damage to the substrate, catalyst particle, and/or tube: it amounts to 1000 K at 100 MΩ for $I = 2$ μA, and will increase with I^2. This resistance is also well within the values measured in the 2P characterization, and estimated from the $I-V$ plots. We can also directly compare Fig. 7 with the

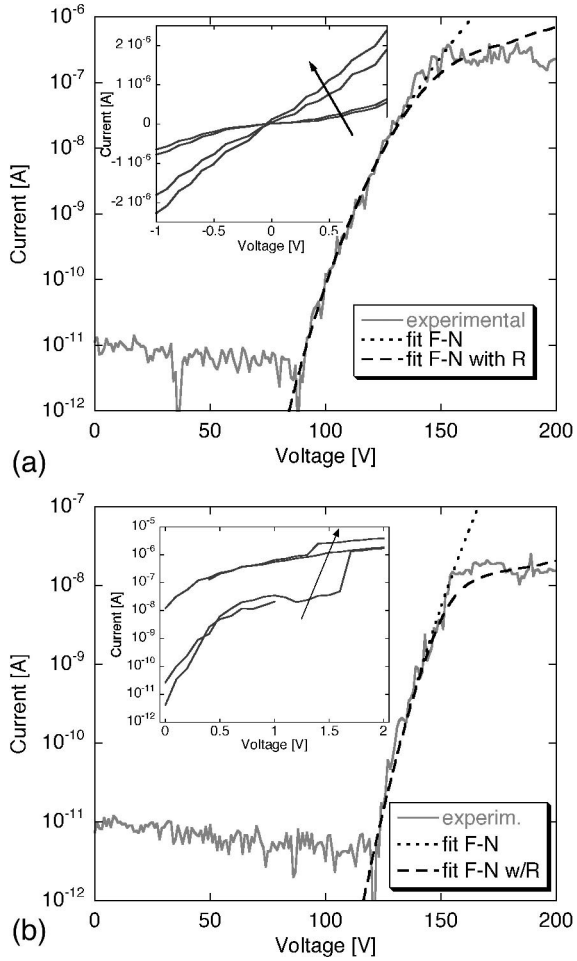

FIG. 8. Field emission $I-V$ curves and corresponding fits to the FN law (dotted lines) and FN law with series resistance (dashed lines), with in inset successive 2P $I-V$ curves (low bias only). (a) 2P characterization after mechanical stressing, but before field emission on a nanotube with $h=1.4\ \mu$m, $r=7.5$ nm, and $d=2.65\ \mu$m. The 2P resistance decreases from 4 MΩ to 500 kΩ with successive measurements at increasing voltage. The fits for the subsequent FE measurements yield $\gamma=90$ and $R=30$ MΩ. (b) 2P characterization after field emission on a nanotube with $h=2.36\ \mu$m, $r=8$ nm, and $d=3.75\ \mu$m. The fits yield $\gamma=65$ and $R=500$ MΩ. The 2P resistance decreases from 200 to 2.7 MΩ with successive measurements at increasing voltage.

failure of Fig. 1 occuring at 9 μA with a resistance of 5 MΩ (as estimated from the $I-V$ curve), leading to a temperature elevation of 2000 K.

One potential problem with this hypothesis appears when 2P and FE measurements on the same emitter are considered. The 2P curves were acquired mostly by sweeping the voltage directly from a negative to a positive voltage value (instead of increasing the voltage from 0 V). An example is shown in Fig. 8(a), with only mechanical stressing with an applied field (no FE) before 2P characterization. The 2P measurements shown in the inset reveal a linear $I-V$ behavior at low bias only, with a resistance of 4 MΩ for the first sweep. Interestingly, the 2P resistance drops sharply as the voltage range of the sweep is increased, reaching a stable and reproducible value of 500 kΩ for the last sweep. The subsequent FE measurements reveal an apparent resistance in series with the emitter of 30 MΩ, which is markedly higher than the 2P value. Conversely, Fig. 8(b) shows the same kind of characterization, but with the FE performed *before* the 2P measurements and by starting the 2P $I-V$ sweeps at 0 V. FE suggests a resistance in series of 500 MΩ, while the 2P resistance is very high in the initial sweep and is estimated to 200 MΩ. A succession of step-like increases in current is observed when the voltage is increased, leading to a decrease of the resistance down to 2.7 MΩ.

From the above results we suggest that the contact (and especially its resistance) is strongly influenced by the measurements. The tensile loading of the emitters during field emission may lead to the rupture of conduction channels at the contact between support and emitter and hence to an increase in resistance, in a manner similar to what happens in mechanically controllable break junctions.[50] Conversely, the contact resistance is ''annealed'' in the 2P mode, as the resistance is lowered by forcing a current through contact and nanotube. In short, the resistance is increased during FE by breaking up mechanically some conduction channels, while these are restored (or others are created) in a 2P characterization. We therefore suggest that the increase in temperature at the contact resistance is enhanced by the mechanical stress due to the applied field before and during field emission, which would elucidate the fact that the FE failure occurs at the contact and not along the tube as in 2P failure.

V. IMPLICATIONS FOR DEVICES

What are the implications of the above findings for field emission devices? The degradation of a film emitter is never abrupt, but gradual and occurs during initial $I-V$ testing[51] as well as during measurements at constant applied voltage over long periods.[5,52] Regarding the first type of degradation, it became obvious from several studies on nanotube arrays that the field emission (FE) properties (e.g., threshold field, field enhancement factor γ) are degraded when the field is ramped up to progressively higher values, which shows as a shift of the $I-V$ curve toward higher fields and a decrease of the field enhancement. One probable cause for this ''training'' effect[51] is the destruction of the leaders, i.e., the nanotubes with the highest field enhancement that dominate field emission at the onset.[47] This problem can be circumvented by systematically operating the emitters at high currents to ensure reproducible characteristics. Even with such precautions, a gradual degradation is also observed when the emitters are operated at constant applied voltage. This degradation is faster for singlewall as compared to arc-discharge multiwall nanotubes[52] but lessens with time, leading to reported lifetimes in excess for 8000 h.[5] The decrease in γ associated with the degradation, as well as the observed decrease in emitter density[42,47] leads one to conclude that this gradual degradation is in fact due to the failure of individual emitters.

In our case, failure under FE occurs at the contact, and this junction between emitter and support is at present a poorly known part of the whole system, be it from a me-

chanical or electrical point of view. Both aspects play a critical role in emitter failure, as demonstrated above. The results available in the literature could lead one to conclude that arc-discharge tubes are the most resilient emitters, which may be a premature conclusion as no study has been conducted yet in a configuration similar to the one employed here (e.g., a nanotube film prepared by a squeeze-paste technique[53]). All degradation experiments on single-wall and arc-discharge multiwall nanotubes have been carried out with nanotubes attached to sharpened wires,[12–14] where the contact is mechanically and electrically strong as the contact area is much higher than in our configuration (see Sec. IV C). The failures witnessed in these cases represent the intrinsic limits of the nanotube emitters, whereas the substrate-emitter system as a whole (typical of a nanotube film used in a practical device) is considered in the present study. An experiment similar to the one described here would be hence needed to directly compare the degradation behavior of nanotubes that are embedded in a conductive resin with emitters directly grown by CVD on a substrate. Although the former solution may warrant a better mechanical contact, at present it lacks the flexibility of CVD for influencing the spacing,[29,54] length,[29,55] and diameter[56] of the nanotubes and hence for tuning the field emission properties.[7]

It appears in any case that the emission of high currents (over 10 μA) will damage CVD and arc-discharge nanotubes. To ensure stable emission and long lifetime, it may hence be favorable to protect actively the emitters against FE failure by including a ballast resistor in series. This will also enhance emission homogeneity and emission site density.[57] It will also be of importance to study more closely the substrate-emitter contact in CVD-grown nanotubes, and to devise methods to enhance the contact.

VI. CONCLUSION

We have studied the failure of multiwall carbon nanotubes field emitters grown by CVD on planar substrates in field emission as well as a two-probe configuration. The failures induced by high currents during 2P characterization led to a sundering of the tube at or near its middle, which is consistent with a local evaporation due to resistive heating. The failure occurred at or near the contact during field emission on our CVD films, which suggests a degradation mechanism that is due either to mechanical failure due to the tensile loading of the emitter under the applied electric field or to resistive heating at the contact that is enhanced by the mechanical stress. We could assign the former cause to failures occurring at applied fields and currents below 4 V/nm and 1 μA, and the latter cause to failures occurring at higher fields and currents.

ACKNOWLEDGMENTS

This work was supported by the European Community and the Federal Office for Education and Science of Switzerland in the frame of the project CANADIS (IST-1999-20590). We acknowledge enlightening discussions with Richard G. Forbes on the mechanical stressing of the emitters during FE, with Kenneth B. K. Teo on stress-induced failure, and with Philippe Lambin on the consequences of mechanical stressing on the electric transport of nanotubes.

*Present address: Rolex S.A., 3-7 rue François-Dussaud, 1211 Genève 24, Switzerland. Electronic address: jean-marc.bonard@a3.epfl.ch; URL: http://ipnwww.epfl.ch/nanotubes.html

[1] Q.H. Wang, A.A. Setlur, J.M. Lauerhaas, J.Y. Dai, E.W. Seelig, and R.P.H. Chang, Appl. Phys. Lett. **72**, 2912 (1998).
[2] W.B. Choi, D.S. Chung, J.H. Kang, H.Y. Kim, Y.W. Jin, I.T. Han, Y.H. Lee, J.E. Jung, N.S. Lee, G.S. Park, and J.M. Kim, Appl. Phys. Lett. **75**, 3129 (1999).
[3] Y.W. Jin *et al.*, J. Appl. Phys. **92**, 1065 (2002).
[4] N. de Jonge, Y. Lamy, K. Schoots, and T.H. Oosterkamp, Nature (London) **420**, 393 (2002).
[5] Y. Saito and S. Uemura, Carbon **38**, 169 (2000).
[6] H. Murakami, M. Hirakawa, C. Tanaka, and H. Yamakawa, Appl. Phys. Lett. **76**, 1776 (2000).
[7] M. Croci, I. Arfaoui, T. Stöckli, A. Chatelain, and J.-M. Bonard, Microelectronic J. (to be published).
[8] R. Rosen, W. Simendinger, C. Debbault, H. Shimoda, L. Fleming, B. Stoner, and O. Zhou, Appl. Phys. Lett. **76**, 1668 (2000).
[9] O. Zhou's group (UNC Chapel Hill) and W. Zhu (Lucent Technologies), pending U.S. patents.
[10] G.Z. Yue, Q. Qiu, B. Gao, Y. Cheng, J. Zhang, H. Shimoda, S. Chang, J.P. Lu, and O. Zhou, Appl. Phys. Lett. **81**, 355 (2002).
[11] M.J. Fransen, T.L. van Rooy, and P. Kruit, Appl. Surf. Sci. **146**, 312 (1999).
[12] J.-M. Bonard, F. Maier, T. Stöckli, A. Châtelain, W.A.D. Heer, J.-P. Salvetat, and L. Forró, Ultramicroscopy **73**, 9 (1998).
[13] Z.L. Wang, P. Poncharal, and W.A. de Heer, Appl. Phys. Lett. **80**, 856 (2002).
[14] K.A. Dean, T.P. Burgin, and B.R. Chalamala, Appl. Rev. Lett. **79**, 1873 (2001).
[15] K.A. Dean and B.R. Chalamala, Appl. Phys. Lett. **75**, 3017 (1999).
[16] Y. Wei, K. Dean, B. Coll, and J. Jaskie, Appl. Phys. Lett. **79**, 4527 (2001).
[17] J.-M. Bonard, K.A. Dean, B.F. Coll, and C. Klinke, Phys. Rev. Lett. **89**, 197602 (2002).
[18] B.F. Coll, K. Dean, Y. Wei, J. Jaskie, and J.-M. Bonard, Appl. Phys. Lett. (to be published).
[19] J.-M. Bonard, K.A. Dean, and B.F. Coll, Nano Lett. (to be published).
[20] J.W. Gadzuk and E.W. Plummer, Rev. Mod. Phys. **45**, 487 (1973).
[21] I. Brodie and C. Spindt, Adv. Electron. Electron. Phys. **83**, 1 (1992).
[22] K.A. Dean and B.R. Chalamala, Appl. Phys. Lett. **76**, 375 (2000).
[23] K. Hata, A. Takakura, and Y. Saito, Surf. Sci. **490**, 296 (2001).
[24] J.W. Luginsland, A. Valfells, and Y.Y. Lau, Appl. Phys. Lett. **69**, 2770 (1996).
[25] A. Bachtold, M. Henny, C. Terrier, C. Strunk, C. Schönenberger, J.-P. Salvetat, J.-M. Bonard, and L. Forró, Appl. Phys. Lett. **73**, 274 (1998).
[26] P. Avouris, Chem. Phys. **281**, 429 (2002).

[27] V. Meunier, P. Senet, and P. Lambin, Phys. Rev. B **60**, 7792 (1999).
[28] P. Collins and P. Avouris, Appl. Phys. A: Mater. Sci. Process. **74**, 329 (2002).
[29] M. Chhowalla, K.B.K. Teo, C. Ducati, N.L. Rupesinghe, G.A.J. Amaratunga, A.C. Ferrari, D. Roy, J. Robertson, and W.I. Milne, J. Appl. Phys. **90**, 5308 (2001).
[30] V. Semet, V.T. Binh, P. Vincent, D. Guillot, K.B.K. Teo, M. Chhowalla, G.A.J. Amaratunga, W.I. Milne, P. Legagneux, and D. Pribat, Appl. Phys. Lett. **81**, 343 (2002).
[31] K.B.K. Teo, presented at the NT'02 conference, Boston College, Boston MA, July 6–11, 2002 (also see http://www.nanoten.com/nt02/).
[32] P.J. de Pablo, E. Graugnard, B. Walsh, R.P. Andres, S. Datta, and R. Reifenberger, Appl. Phys. Lett. **74**, 323 (1999).
[33] A. Bachtold, M.S. Fuhrer, S. Plyasunov, M. Foreor, E.H. Anderson, A. Zettl, and P. McEuen, Phys. Rev. Lett. **84**, 6082 (2000).
[34] M. Ahlskog, presented at the NT'02 conference, Boston College, Boston MA, July 6–11, 2002 (also see http://www.nanoten.com/nt02/).
[35] W.W. Dolan, W.P. Dyke, and J.K. Trolan, Phys. Rev. **91**, 1054 (1953).
[36] S.T. Purcell, P. Vicent, C. Journet, and V.T. Binh, Phys. Rev. Lett. **88**, 105502 (2002).
[37] M. Sveningsson, presented at the NT'02 conference, Boston College, Boston MA, July 6–11, 2002 (also see http://www.nanoten.com/nt02/).
[38] P. Kim, L. Shi, A. Majumdar, and P.L. McEuen, Phys. Rev. Lett. **87**, 215502 (2001).
[39] W. Yi, L. Lu, l. Zhang Dian, Z.W. Pan, and S.S. Xie, Phys. Rev. B **59**, R9015 (1999).
[40] J. Vanderlinde, *Classical Electromagnetic Theory* (Wiley, New York, 1993).
[41] C.J. Edgcombe and U. Valdré, Philos. Mag. B **82**, 987 (2002).
[42] L. Nilsson, O. Groening, P. Groening, O. Kuettel, and L. Schlapbach, J. Appl. Phys. **90**, 768 (2001).
[43] M.-F. Yu, O. Lourie, M.J. Dyer, K. Moloni, T.F. Kelly, and R.S. Ruoff, Science **287**, 637 (2000).
[44] W.P. Dyke, J.K. Trolan, E.E. Martin, and J.P. Barbour, Phys. Rev. **91**, 1043 (1953).
[45] R. Gomer, Surf. Sci. **299/300**, 129 (1994).
[46] A.T. Sowers, B.L. Ward, S.L. English, and R.J. Nemanich, J. Appl. Phys. **86**, 3973 (1999).
[47] L. Nilsson, O. Gröning, P. Gröning, and L. Schlapbach, Appl. Phys. Lett. **79**, 1036 (2001).
[48] FREEFEM+ is an implementation of a language dedicated to the finite element method that provides a way to solve Partial Differential Equations (PDE). Also see http://www.freefem.org
[49] D.R. Lide, *CRC Handbook of Chemistry and Physics*, 71st ed. (CRC Press, Boca Raton, FL, 1990).
[50] J. van Ruitenbeek, in *Metal Clusters on Surfaces: Structure, Quantum Properties, Physical Chemistry* (Springer-Verlag, Heidelberg, 2000).
[51] J.-M. Bonard, N. Weiss, H. Kind, T. Stöckli, L. Forró, K. Kern, and A. Châtelain, Adv. Mater. **13**, 184 (2001).
[52] J.-M. Bonard, J.-P. Salvetat, T. Stöckli, W.A.D. Heer, L. Forró, and A. Châtelain, Appl. Phys. Lett. **73**, 918 (1998).
[53] D.S. Chung, W.B. Choi, J.H. Kang, H.Y. Kim, I.T. Han, Y.S. Park, Y.H. Lee, N.S. Lee, J.E. Jung, and J.M. Kim, J. Vac. Sci. Technol. B **18**, 1054 (2000).
[54] H. Kind, J.-M. Bonard, C. Emmenegger, L.-O. Nilsson, K. Hernadi, E. Maillard-Schaller, L. Schlapbach, L. Forró, and K. Kern, Adv. Mater. **11**, 1285 (1999).
[55] M. Croci, J.-M. Bonard, O. Noury, T. Stöckli, and A. Chatelain, Chem. Vap. Deposition **8**, 89 (2002).
[56] J.-M. Bonard, P. Chauvin, and C. Klinke, Nano Lett. **2**, 665 (2002).
[57] J. Dijon, A. Fournier, B. Montmayeul, D. Zanghi, B. Coll, I. Arfaoui, J.-M. Bonard, and A.-M. Bonnot (unpublished).